



## INTEGRAL AND DIFFERENTIAL FORMULATIONS APPLIED TO ANALYSIS FLOW OVER A WIND ROTORS

**Rafael Romão da Silva Melo**

**João Marcelo Vedovoto**

**Aristeu da Silveira Neto**

Universidade Federal de Uberlândia

faelromelo@gmail.com, jmvedovoto@mecanica.ufu.br, aristeus@mecanica.ufu.br

**Abstract.** *This paper presents the coupling between two distinct formulations applied to flow analysis of wind rotors, integral and differential formulations. First, for the integral formulation is defined a control volume where the variables problem are defined, as well as necessary working hypothesis, then a proposed mathematical modeling is defined. A major drawback of the integral formulation is the necessity of experimental data (drag and lift coefficient). The differential formulation is used to circumvent this problem, by means of CFD simulations. Simulations through NACA airfoils are performed for to evaluate drag and lift coefficients, to be used then in the integral formulation. The Navier-Stokes equations are solved in house and the Smagorinsky turbulence model with Van Driest damping function is retained. The computational code is implemented with structured cartesian mesh, where the airfoil is modeled using the Immersed Boundary Methodology. The results of simulation through a NACA0012 airfoil are shown for several attack angles and  $Re = 10000$ . Results of energetic efficiency are presented for a horizontal axis wind turbine using the integral formulation, where the coefficients are given by differential formulation.*

**Keywords:** *Integral Formulation, Differential Formulation, Wind Turbine, Immersed Boundary, Numerical Solution*

### 1. INTRODUCTION

One of the steps in search of the best energy efficiency of the turbine is the analysis of the flow around the blades, where the slightest variation in the geometry causes a change in the power generated. To solve this problem in fluid mechanics, an example of fluid structure interaction, is possible to use two different methods, the theoretical model and the experimental model.

The laboratory experiments have the advantage of working with real or approximate configuration of the physical model, but generally an experiment has high cost and presents great difficulty in reproducing the real conditions, for example, simulations at high heights and wind speeds with large variations. This high cost occurs by the necessity to invest in a research laboratory with minimum requirements for testing, and also by the necessity to produce a new prototype for each model designed.

The theoretical analysis for the problem can be choose between two methods: the integral and differential method. The integral method analyzes the problem in a control volume which the wind turbine is immersed, performing an energy balance in this control volume, calculating the power generated from data such as wind speed, angular velocity and profile of the blade of the rotor (Melo and Silveira-Neto, 2012). As this method only works with global parameters, so it's not possible to know in detail at each point in the space around the wind generator, only restricted data in the input and output of the control volume.

The differential method is a powerful tool, allowing to simulate and visualizing in detail what occurs around a body immersed in a fluid, in this case a wind turbine in the current. For this we use the Computational Fluid Dynamics (CFD), which is the area of the scientific computing which uses computational methods for simulating problems involving fluid motion with or without heat transference. The partial differential equations which govern the fluid motion are discretized, and then this equations are solved using computational tools.

In the present work has as objective to apply the two theoretical forms to solve a problem in fluid mechanics, the integral and differential formulations applied in a complex system, in this case wind turbines.

### 2. INTEGRAL FORMULATION

To determine the power generated by the rotor is necessary to determine the forces acting on the blades. In this formulation are used two methodologies, the Blade Element Theory, or BEM (Lanzafame and Messina, 2010; Sedaghat and Mirhosseini, 2012), and the Balance of Linear Momentum.

**2.1 Blade element theory**

The blade element theory is a way of determining the forces acting on the turbine, which are the lift  $F_l$  and drag  $F_d$  forces. For this the blade is divided into a discrete number of elements or planes which the forces are determined. In this theory adopts that the flow of each element is two-dimensional, i.e., there is only the normal (direction of flow) and tangential (direction of the rotation of the turbine) components of velocity, so the component of the velocity in the radial direction is null.

The Fig. 1 presents a blade of a HAWT with radius  $R$ , whose a generic element has radius  $r$ . When the free wind speed  $U_\infty$  approaches this blade element, it's reduced to a slower speed, known  $U_n$ . Then at a distant point from the turbine the wind speed becomes  $U_2$ . And in this element there is the tangential velocity  $U_t$  due to rotation of the turbine, which rotates with angular velocity  $\omega$ . This figure also shows that each blade element has different length of chord  $c$  and a twist angle  $\lambda$ , which is the angle formed between the chord direction and the tangential direction of the element.

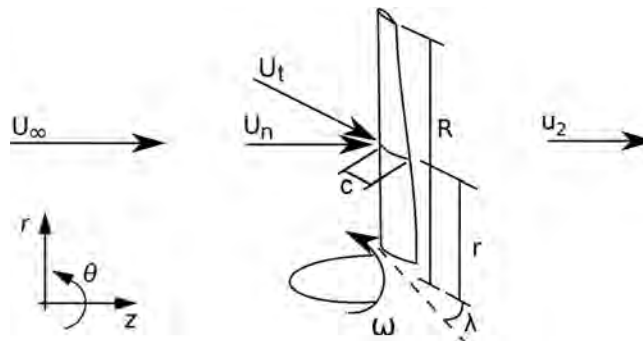


Figure 1. Geometric characteristics of a blade of a HAWT and a generic plan for analysis using the BEM.

The Fig. 2 shows a diagram representing a plan of a blade element. This figure shows that this element with chord length  $c$  and twist angle  $\lambda$  is reached by two velocities, the normal  $U_n$  and tangential  $U_t$  velocity. The resulting velocity  $V$  on the element is the vector sum of this two velocities. The angle of attack  $\alpha$  is formed between the resulting velocity  $V$  and the line of the chord  $c$ . Another important variable presented in this diagram is the angle of flux  $\phi$ , formed between the resultant velocity  $V$  and tangential direction. Finally this figure shows the drag force  $F_d$  in the direction of the velocity  $V$ , and lift forced  $F_l$ , perpendicular to the drag force.

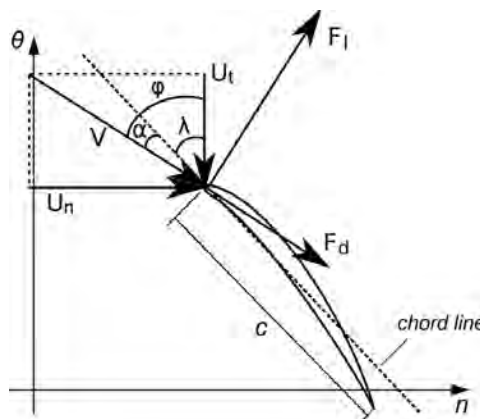


Figure 2. Diagram of velocities and forces acting on a generic blade element.

For this control volume is defined two induction factors: the axial induction factor  $a$ , proportional to  $U_\infty$ , and tangential induction factor  $a'$ , proportional to  $\omega r$ . Higher is  $a$ , lower will be  $U_n$ , and higher is  $a'$ , higher will be  $U_t$ . Knowing the correct velocities,  $U_n$  and  $U_t$ , the forces  $F_l$  and  $F_d$  can be calculated.

The complete mathematical model applied in each blade element is presented below:

1. Estimate the induction factors. For example,  $a = 0.1$  and  $a = 0.01$
2. Calculate the normal and tangential velocities.

$$U_n = U_\infty - aU_\infty = U_\infty (1 - a), \tag{1a}$$

$$U_t = \omega R + a'\omega R = \omega R (1 + a'). \tag{1b}$$

3. Calculate the resulting velocity, angle of flow and angle of attack.

$$V = \sqrt{U_n^2 + U_t^2}, \quad (2a)$$

$$\varphi = \arctan\left(\frac{U_n}{U_t}\right), \quad (2b)$$

$$\alpha = \varphi - \lambda. \quad (2c)$$

6. From experimental data obtain the lift  $C_l$  and drag  $C_d$  coefficients for this blade element.

7. Knowing the lift  $C_l$  and drag  $C_d$  coefficients, calculates the coefficients in the normal  $C_n$  and tangential  $C_t$  direction.

$$C_n = C_l \cos(\varphi) + C_d \sin(\varphi), \quad (3a)$$

$$C_t = C_l \sin(\varphi) - C_d \cos(\varphi). \quad (3b)$$

8. Calculate the differential force in the normal  $dF_n$  and tangential  $dF_t$  directions for this blade element.

$$dF_n = BC_n \frac{1}{2} \rho V^2 c dr, \quad (4a)$$

$$dF_t = BC_t \frac{1}{2} \rho V^2 c dr, \quad (4b)$$

where  $\rho$  is the fluid density,  $B$  is the number of blades of the turbine,  $c$  and  $dr$  the chord length and the length of the depth of the blade element, respectively.

With the blade element theory we can calculate the forces on all blade elements, i.e., all forces acting on the turbine. But the induction factors aren't known, then it's necessary to find a new alternative, which will be presented in the next subsection.

## 2.2 Balance of Linear Momentum

Another way of calculating the normal and tangential forces at each point of the blades is through the theory of Balance of Linear Momentum in a control volume determined. The Fig. 3 shows a control volume in the form of a ring, where the radius of the rotor is divided into a finite number of elements of length  $dr$ . This length runs a circular section, as seen in Fig. 3.a, encompassing the blade elements of the BEM theory for all blades in the generic radius  $r$ , where the differential forces acting in the normal  $dF_n$  and tangential  $dF_t$  directions on that control volume has the same value of the differential forces of the previous theory (BEM). This control volume in the normal direction is not cylindrical, but follows a curve defined by two streamsurfaces, closing this volume of control as seen in Fig. 3.b. The entry of fluid in this control volume starts in the plane 1, where the flow velocity is the velocity of the free wind speed  $U_\infty$ , and the pressure is atmospheric pressure. On the plane 2 the flow velocity is uniform and equal to  $u_2$ , and the pressure also is the atmospheric pressure. Since the pressure input and the output are equal, there is no resultant force due to pressure on this control volume.

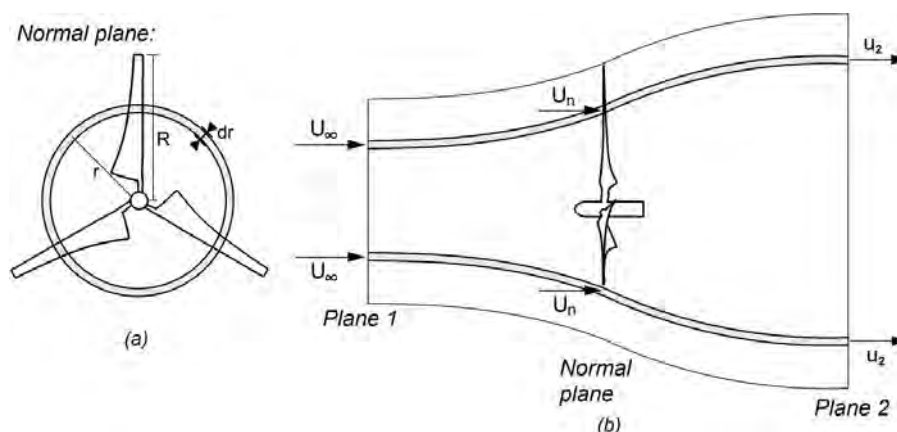


Figure 3. Control volume in the form of an annular ring

To determine the differential forces in normal  $dF_n$  and tangential  $dF_t$  directions applies the balance of linear momentum in both directions, obtaining the following equations, also in function of the induction factors  $a$  and  $a'$ :

### 1. Normal direction:

$$dF_n = \rho U_\infty^2 a (1 - a) 4\pi r dr. \quad (5)$$

### 2. Tangential direction:

$$dF_t = \omega r \rho U_\infty a' (1 - a) 4\pi r dr. \quad (6)$$

### 2.3 Coupling between the two theories

Once the two equations are determined for the differential force in the normal direction  $dF_n$  (Eqs. (4a) and (5)) and tangential direction  $dF_t$  (Eqs. (4b) and (6)), we can equate them in order to find the induction factors  $a$  and  $a'$ .

Equating the Eqs. (4a) and (5), and Eqs. (4b) and (6), we obtain two expressions for the two induction factors:

$$a = \sigma_r C_n \frac{V^2}{U_\infty^2} \frac{1}{4(1-a)}, \quad (7a)$$

$$a' = \sigma_r C_t \frac{V^2}{\omega r U_\infty} \frac{1}{4(1-a)}, \quad (7b)$$

where the strength  $\sigma_r = \frac{Bc}{2\pi r}$  represents the ratio between the chord area of all the blades over the area of the circular disk.

As the induction factors are in function of the variables calculated with estimated values for these factors, we must iterate to converge to the correct result, replacing the random induction factors estimated by factors calculated by Eqs. 7a and 7b.

## 3. DIFFERENTIAL FORMULATION

This section will be present two mathematical formulations used in the differential formulation: Eulerian formulation, which models the equations for the continuous domain of fluid, with the motion and turbulence equations, and the Lagrangian formulation, which models the equations for the immersed boundary method, used to represent bodies in domain of fluid.

### 3.1 Eulerian formulation

In the eulerian formulation the calculation domain is modeled as if it were occupied by fluid. This domain is represented by the Navier-Stokes equation, as shown below:

$$\frac{\partial(\rho u_i)}{\partial t} + \frac{\partial(\rho u_i u_j)}{\partial x_j} = -\frac{\partial p}{\partial x_i} + \frac{\partial}{\partial x_j} \left[ \mu \left( \frac{\partial u_i}{\partial x_j} + \frac{\partial u_j}{\partial x_i} \right) \right] + f_i, \quad (8)$$

where  $p$  is the pressure,  $\rho$  is the fluid density,  $u_i$  is the component  $i$  of the velocity vector, and  $f_i$  is the component  $i$  of the eulerian force field which the immersed boundary method with complex geometry can be represented.

And the model must obey the continuity equation:

$$\frac{\partial \rho}{\partial t} + \frac{\partial(\rho u_i)}{\partial x_i} = 0. \quad (9)$$

This work is used the Smagorinsky turbulence model, which is based on the assumption of local equilibrium between the small scales (production of turbulent kinetic energy is equal the dissipation in this small scales). The eddy viscosity can be expressed as a function of the strain rate tensor  $S_{ij}$ , the length scale  $\Delta$  and a constant  $C_s$ , known as constant of Smagorinsky:

$$\nu_t = (C_s \Delta)^2 \sqrt{2S_{ij}S_{ij}}. \quad (10)$$

The strain rate tensor  $S_{ij}$  is given by

$$S_{ij} = \frac{1}{2} \left( \frac{\partial \bar{u}_i}{\partial x_j} + \frac{\partial \bar{u}_j}{\partial x_i} \right), \quad (11)$$

and the length scale  $\Delta$  is usually calculated as a function of the mesh discretization:

$$\Delta = \sqrt[3]{\Delta x \Delta y \Delta z}. \quad (12)$$

VanDriest (1956) proposed a damping function, which can be applied with Smagorinsky constant. This function is given by

$$C_s = C_{so} \left( 1 - e^{-d^+ / A^+} \right)^2, \quad (13)$$

where  $d^+ = du_\tau / \nu$  is the relative distance,  $d$  is the distance between the the volume Eulerian analyzed and the nearest wall,  $u_\tau = \sqrt{\tau_w / \rho}$  is the shear rate,  $\tau_w$  is the shear stress,  $A^+ = 25$  is a constant determined by Ferziger and Peric (1996) and  $C_{so}$  is the Smagorinsky constant, usually limited to  $0.05 \leq C_{so} \leq 0.3$ .

The variables of this damping function for modeling the immersed boundary are defined as follows:  $d$  is the distance from the center of the eulerian volume to the center of the nearest lagrangian volume, and the  $\tau_w$  tension is calculated from the velocity vector  $(v_x, v_y, v_z)$  of the eulerian volume where the center of the lagrangian volume is immersed, which is the nearest lagrangian volume of the eulerian volume analyzed.

For calculate the  $\tau_w$  is necessary to project the velocity vector  $(v_x, v_y, v_z)$  in the normal direction of the immersed boundary. By linear algebra the projected vector  $(v_{xPro}, v_{yPro}, v_{zPro})$  is given by:

$$\begin{bmatrix} v_{xPro} \\ v_{yPro} \\ v_{zPro} \end{bmatrix} = \left\{ \begin{pmatrix} 1 & 0 & 0 \\ 0 & 1 & 0 \\ 0 & 0 & 1 \end{pmatrix} - \begin{bmatrix} n_x \\ n_y \\ n_z \end{bmatrix} \begin{bmatrix} n_x & n_y & n_z \end{bmatrix} \right\} \begin{bmatrix} v_x \\ v_y \\ v_z \end{bmatrix}, \quad (14)$$

where  $(n_x, n_y, n_z)$  is the component of the unit normal vector of the lagrangian volume in three directions.

And finally  $\tau_w$  is calculated by Eq. 15.

$$\tau_w = \mu \frac{\sqrt{v_{xPro}^2 + v_{yPro}^2 + v_{zPro}^2}}{\sqrt{\Delta x^2 + \Delta y^2 + \Delta z^2}}, \quad (15)$$

where  $(\Delta x, \Delta y, \Delta z)$  is the dimensions of the eulerian volume where the center of lagrangian volume is contained.

### 3.2 Lagrangian formulation

In the immersed boundary method is used a independent mesh to define the body in fluid. One of the main advantages is the possibility to simulate flow over complex geometries.

The force term  $f_i$  of the equation of linear momentum defines the interface immersed. To calculate this force it's used a distribution function:

$$f_i(\vec{x}) = \sum_K \vec{F}(\vec{x}_K) D_{ij}(\vec{x} - \vec{x}_K) \Delta V(\vec{x}_K), \quad (16)$$

where  $\Delta V(\vec{x}_K)$  is the volume of the lagrangian element and  $D_{ij}$  is a function interpolation/distribution. In this work, we adopted the hat function, which has the following form:

$$D_{ij}(\vec{x}_K) = g(x_K - x_i) g(y_K - y_j) g(z_K - z_k). \quad (17)$$

$$g(r) = \begin{cases} \frac{1 - \|r\|/\Delta}{\Delta} & , \|r\| \leq \Delta \\ 0 & , \|r\| > \Delta \end{cases}. \quad (18)$$

where  $\Delta$  the characteristic size of the eulerian mesh. This function shows that further are the eulerian volume of the lagrangian point, lower are the value of the distributed force at those volume.

Finally  $\vec{F}(\vec{x}_K)$  represents the force in the lagrangian point, which will be distributed in the eulerian field, delimiting the immersed boundary. As in the all calculating domain, the equation of momentum is valid in each lagrangian point, respecting the continuum hypothesis, since these points are immersed in the eulerian field. So rewriting the equation 8 for

each lagrangian point, applying a discretization in the temporal term, adding and subtracting one auxiliary parameter  $U^*$  and using the superposition principle, the obtained equation which is solved in two parts:

$$\frac{U_i^* - \alpha_1 U_i^t + \alpha_0 U_i^{t-\Delta t}}{2\Delta t} + R H S_i^t = 0, \quad (19a)$$

$$F_i(\vec{X}, t) = \frac{\alpha_2 U_i^{t+\Delta t} - U_i^*}{\Delta t}, \quad (19b)$$

where  $U_i^{t+\Delta t}$  is the desired velocity for the body. If the immersed boundary is stationary, the value of  $U_i^{t+\Delta t}$  is null. If the boundary is moving, these value is equal to the velocity of the body. For the calculation of  $U_i^*$ , it's used the Eq. (20):

$$U_i^* = \sum_{\Omega} u_i^* D_h(x_i - x_K) h^3, \quad (20)$$

where  $D_h$  is represented by a function interpolation/distribution,  $u^*$  is the eulerian velocity at the lagrangian point and  $h$  is the distance between two lagrangian points.

In short, the multi direct forcing calculate the velocity in lagrangian point, then calculate the force in this point, and finally this force is distributed in the eulerian domain. This procedure is performed in an iterative process until the force converge to a value with minimal residue, for all time steps.

## 4. RESULTS AND DISCUSSION

### 4.1 Results of the integral formulation

To apply the full modeling will be used geometric and experimental data of the wind turbine OWW, 250 kW , installed in the testing area of the Brazilian Center for Wind Energy, in Olinda (Leite and Araújo, 2007). The Fig. 4 shows the length of the chord  $c$  and the twist angle  $\lambda$ , in function of the radius  $r$ .

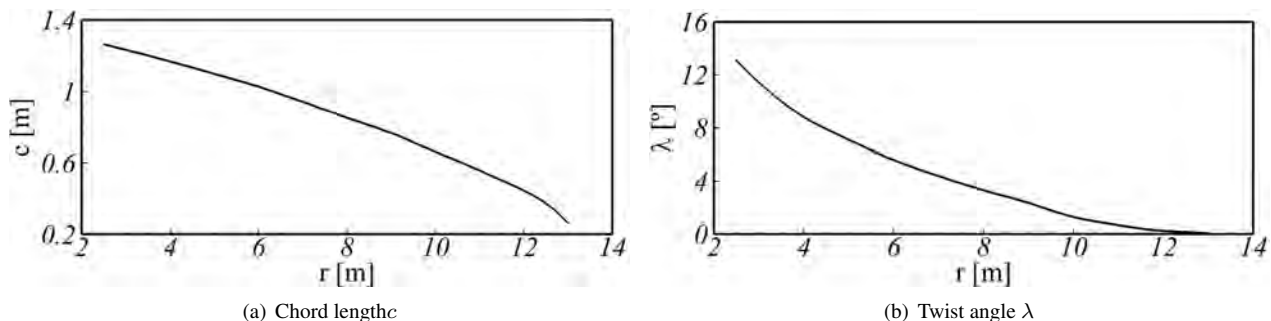


Figure 4. Geometric data of the blade of the OWW turbine in function of the ray  $r$  (Leite and Araújo, 2007).

The Fig. 5 presents the curves of the lift  $C_l$  and drag  $C_d$  coefficients as function of angle of attack for the profile used in the turbine OWW (Leite and Araújo, 2007). These coefficients will be used in the full model.

It was simulated different conditions of flow, where the tip speed ratio  $tsr$ , which is the ratio between the velocity  $wR$  of the blade tip and the free stream wind  $U_\infty$ , varies between 1 and 11. This range often is the operational range of a horizontal axis wind turbine. Was considered rotor with 3 blades, very common in wind farms. To vary the speed ratio  $tsr$  was set wind speed  $U_\infty = 7.0 \text{ m/s}$  and it was varied and the angular velocity  $\omega$  of the turbine. Finally it was considered the air density,  $\rho = 1.225 \text{ Kg/m}^3$ .

Following are the results obtained with the iterative method proposed in the integral formulation. To understand what happens with the variables of the problem are presented results for four different  $tsr$ , between  $tsr = 1$  and  $tsr = 4$ , ranging from 1 to 1.

The Fig. 6 presents the induction factors  $a$  e  $a'$  in function of the dimensionless radius of the blade  $r/R$ , where  $r$  is the distance from the base of the blade to the point of analysis and  $R$  is the total radius of the blade. Note that the axial induction factor  $a$  follows the trend of decrease as the radius increases, except for the case where  $tsr = 4$ , which the curve decreases and then increases again to a peak and decrease again. The axial induction factor  $a$ , i.e., the deceleration of the free stream wind  $U_\infty$  is greatest at the base of the blade, probably due to the robustness of this part, a region where the profiles have the greatest chord length. This deceleration tends to increase along the radius as the angular velocity of the turbine increases. It can also be noted that the factor  $a$  is lower in the tip region of the blade, where the chord length is reduced. The tangential induction factor  $a'$  shows that the increased of the velocity in the tangential direction due the

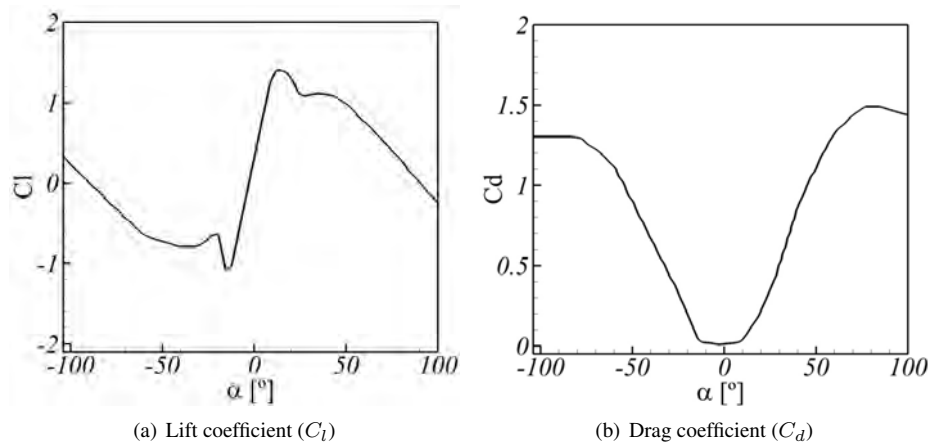


Figure 5. Experimental coefficient as a function of angle of attack  $\alpha$  for the profile of the turbine OWW for various Reynolds numbers (Leite and Araújo, 2007).

rotation of the turbine is greater at the base of the blade, and tends to decrease with an exponential characteristic along the radius. This occurs because in the base of the blade the chord is greater and the angle of twist is also increased, resulting in a bigger injection of angular momentum into the fluid close to the axis of the rotor, and further due to the robustness of this part of the blade.

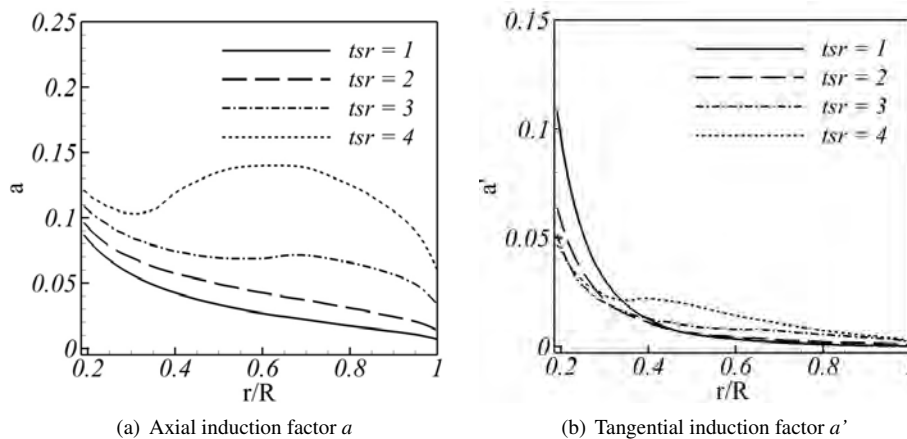


Figure 6. Induction factors in function of  $r/R$  for various values of  $tsr$ .

The Fig. 7 shows the differential force acting on each blade element in the normal direction  $dF_n$  and tangential direction  $dF_t$  of the turbine. Note that for both forces, higher is the angular turbine, greater is the force on each element. Forces are directly proportional to the resulting velocity, which increases with the radius, and inversely proportional to the chord length  $c$ , which decreases with radius. Thus, for each  $tsr$  the point of greatest force, in the normal and tangential direction, is in a position in the center of the blade. At the base of the blade the forces are smaller due to the lower velocity, and these forces are also smaller in blade tip because it has the minimum chord length.

With the correct values of the induction factors it's possible to calculate the true values for the forces acting in all points of the blade. Multiplying the differential force in tangential direction by the local radius, we obtain the torque on each blade element. Adding the torque of all elements obtain the total torque. Multiplying this torque by the angular velocity of the turbine obtain the power. And finally dividing this power by the total variation of the kinetic energy of the wind that reaches the turbine we obtain the power coefficient, which is shown in Fig. 8. This curve follows the trend of a rotary machine, starting with low power at smaller velocities. As the velocity increases, the power coefficient also increases, reaching a point of maximum efficiency. In this case, the coefficient reaches the maximum of  $C_p = 0.48$  for the tip speed ratio  $tsr = 7$ . After this point of maximum efficiency the curve decay, which can reach negative values for high speeds. The power coefficient curve as a function of speed ratio  $tsr$  it's important to define the range of operation of the turbine. With this information it's possible design and control the turbine for this operates in the range of  $tsr$  with greater efficiency.

The objective of this work isn't to propose a configuration of wind turbine looking a greater efficiency, but the Fig. 9 presents an example of change that is possible to do in the design of a wind rotor in search of a better energetic harnessing. This figure shows the curve of the power coefficient as a function of  $tsr$  for turbine with different numbers of blade. It

R. R. S. Melo, J. M. Vedovoto and A. Silveira Neto  
Integral and Differential Formulations Applied to Analysis Flow Over a Wind Rotors

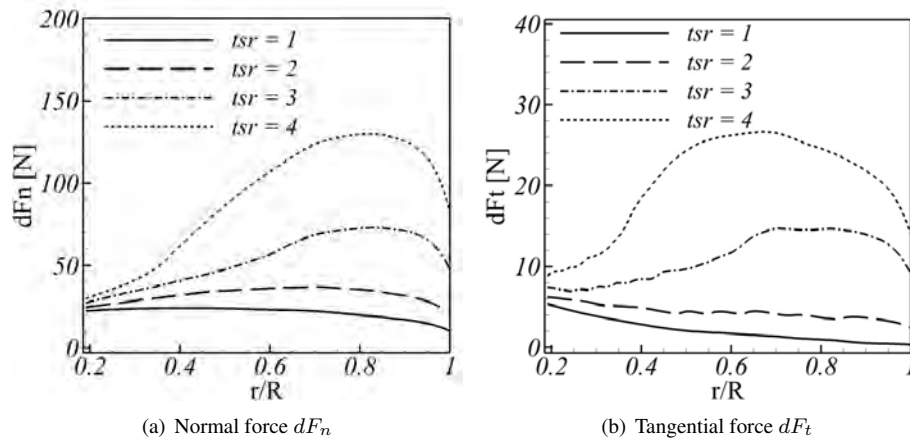


Figure 7. Normal and tangential forces acting on the blade for different values of  $tsr$ .

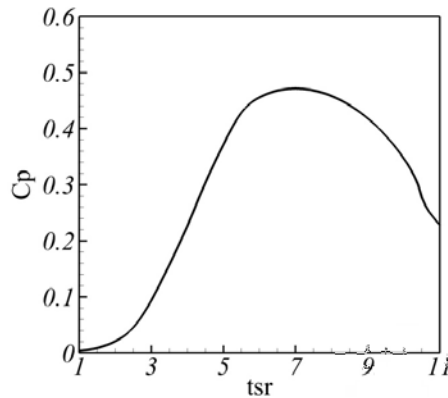


Figure 8. Power coefficient  $C_p$  in function of  $tsr$ .

was used turbines with different numbers of blades, varying from 1 to 6. Note that the turbine with one blade presents a bigger operating range, but has a maximum peak of power lower compared with the other configurations. From the turbine with one blade to turbines with three blade the maximum value of power coefficient increases, but the operating range decreases. The turbine with four blade compared with the three bladed does not increase the power significantly, but occurs a reduction in the operating range. Turbine with blade number greater than four reduces the power coefficient and operating range. So, it's noted that the most suitable configuration for this turbine is to utilize turbine with three blades, looking for maximum efficiency and still has a relatively large operating range. This can be noticed in practical, since most wind farms have turbines with three blades.

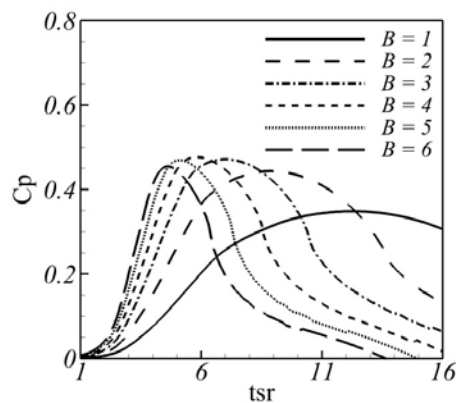


Figure 9. Power coefficient  $C_p$  in function of  $tsr$  for turbine with different numbers of blades.

## 4.2 Flow around the aerodynamic profile NACA 0012

In the simulation of the aerodynamic profile was used the profile NACA 0012, a symmetric profile in respect to the chord line. In order to capture more detail in flow, it's was performed a two-dimensional simulation, seeking a higher level of refinement around the geometry with a moderate cost. Cartesian mesh was used with dimensions of  $9.0\text{ m}$  in  $x$  and  $5.0\text{ m}$  in  $y$ . This mesh has three distinct refinements in each direction: a region more refined and uniform, which is bounded by two regions with less refined and non-uniform, totaling 9 regions with different refinements. The fig. 10 describes in detail the amount of eulerian volumes used in each region, with their lengths, totaling 208.800 Eulerian volumes and totaling 402 lagrangian elements. It's used a Reynolds number  $Re = 10^4$ , with the Smagorinsky turbulence model.

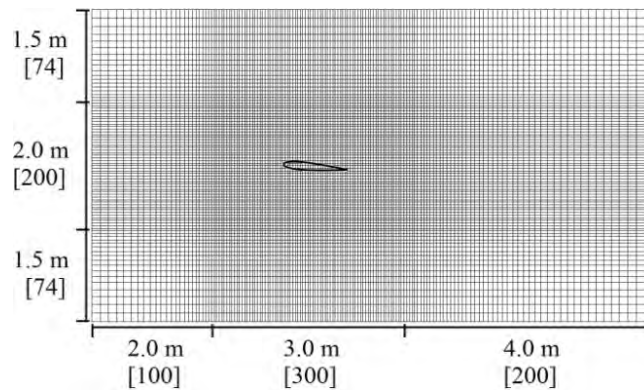


Figure 10. Eulerian mesh used for the airfoil simulation.

The Fig. 11 presents the temporal evolution of the flow from the initial time with angle of attack  $\alpha = 5^\circ$ . Note that for the initial instant the streamlines are aligned with the profile, once the initial condition of the flow is a constant velocity in the direction  $x$ . As the time increases occurs the detachment of the boundary layer, as evidenced by the formation of a vortex, originating a street, known as Von Karman Street. For this angle of attack is expected that the boundary layer don't happen the detachment after the transition of the flow, but this isn't occurs in this case, as can be noted in the last stages shown in this figure.

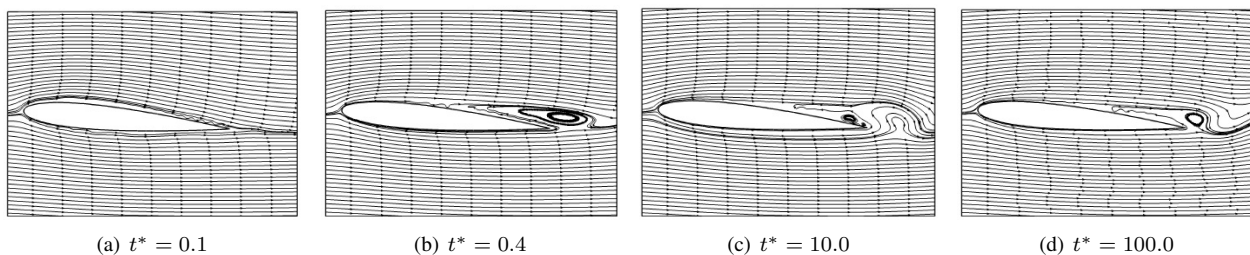


Figure 11. Temporal evolution of the flow around the profile with  $\alpha = 5^\circ$ .

To make an analysis quantitative analysis of the results obtained from the simulations will be presented the drag and lift coefficients, compared with values obtained from the literature.

The Fig. 12 shows the lift and drag coefficients as a function of angle of attack compared with the literature (Drela, 1989; Akbari and Price, 2003; Oliveira, 2006). Drela (1989) presents the XFOIL, a public domain code (GNU) for design and analysis of airfoils. Akbari and Price (2003) presents the Vortex-Lattice method. Oliveira (2006) solves the Navier-Stokes equations with cartesian mesh and uses the immersed boundary methodology through the virtual physical model. The drag curve follows the trend of increase as the angle of attack  $\alpha$  is increased, but for all angles of attack found coefficient is above the literature data, indicating that there is an excess of force compared with these references. It's expected that he curve of lift coefficient for angle of attack between  $0^\circ$  and  $15^\circ$  increase linearly, but this isn't observed in the obtained results. For angle of attack up to approximately  $8^\circ$ , the lift oscillates around a increasing line. For angles greater than  $8^\circ$  there is a very large increase of this curve, and then stabilizes at a approximate value of  $C_l = 0.8$ .

Some factors that contributes to this problem and possible solutions are discussed below. The factor that really changes the coefficients is the premature detachment of the boundary layer, detachment observed previously. A factor that can cause this detachment is the Smagorinsky turbulence model, which creates a high viscosity on the immersed boundary. Searching to solve this problem, will be used the Van Driest damping function.

The Fig. 13 presents the temporal evolution of the flow for the angle of attack  $\alpha = 5^\circ$ , but now using the Van Driest damping function. Note that the flow at the initial time is aligned with the profile, and with the course of time occurs the

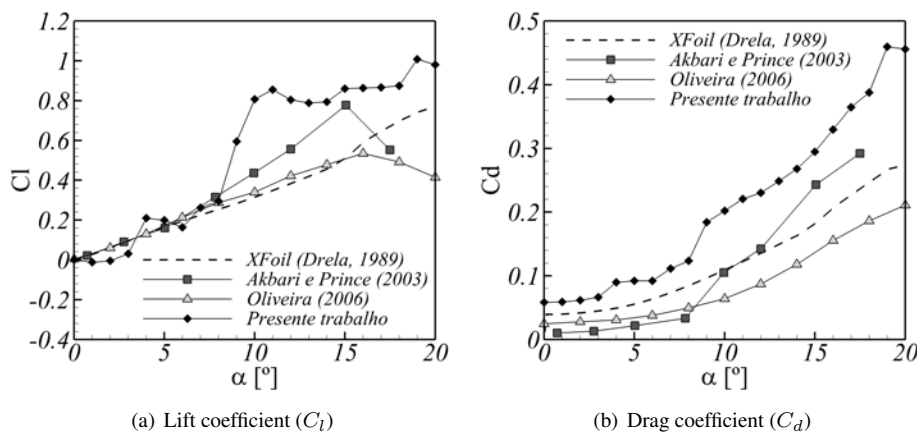


Figure 12. Lift and drag coefficients in function of the angle of attack  $\alpha$ .

detachment of boundary layer and the creating of a vortex structure. However with the damping function there isn't the detachment of the boundary layer when it reaches steady state.

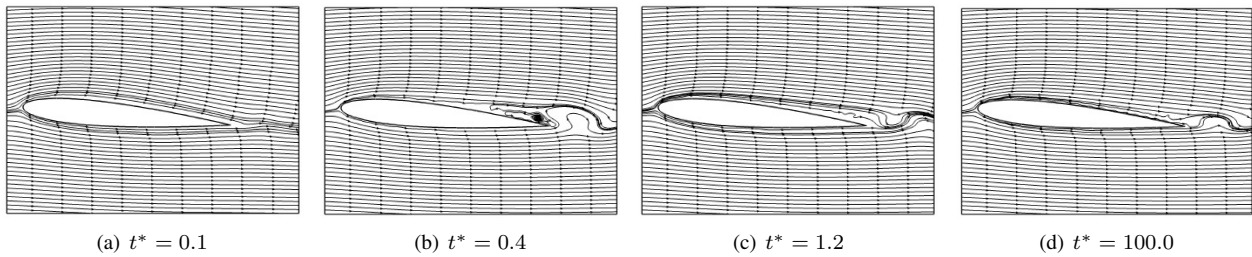


Figure 13. Temporal evolution of the flow around the profile with  $\alpha = 5^\circ$  using the Van Driest function.

The Fig. 14 presents the temporal evolution of the flow for the angle of attack  $\alpha = 10^\circ$ . This figure shows clearly the detachment of the boundary layer by the formation of multiple vortices, which occur in the profile. Analyzing the immersed boundary notes the consistency of the flow around the geometry, even for a instability flow with high Reynolds number, the streamline don't cross the surface. The vortices are formed respecting the indirectly no slip condition, imposed by the methodology.

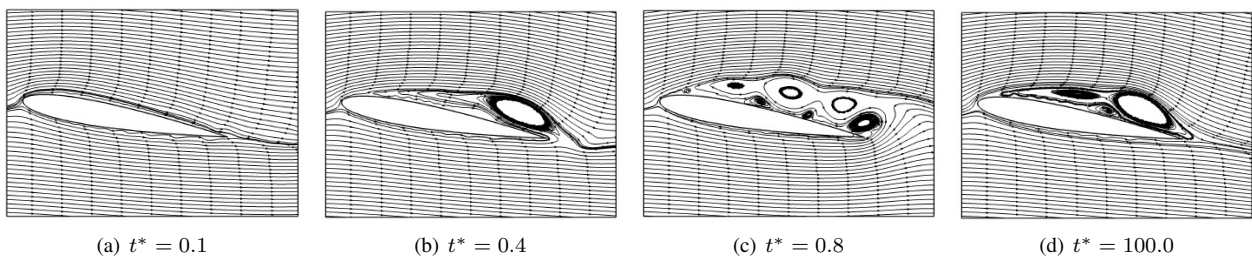


Figure 14. Temporal evolution of the flow around the profile with  $\alpha = 10^\circ$  using the Van Driest function.

The Fig. 15 shows the drag  $C_d$  and lift  $C_l$  coefficients for different angle of attack  $\alpha$ . Note that the curve of lift and drag are closer when compared with the results collected in the literature, previously shown in Fig. 12. The coefficients for angles of attack below  $\alpha = 6^\circ$  follow the curves of the references. The drag remains low and lift increases approximately linear. For angles of attack greater than  $6^\circ$  a fluctuation occurs in the curves, probably because even occur the detachment of the boundary layer for this high angles. Once the literature presented results with references averages equations, a possibility be happening the premature detachment of the boundary layer is due to the turbulence modeling used. Although it's used a damping function in the wall, there are still large fluctuations in the velocity because it's a large eddy simulation. Oliveira (2006) also performs simulations using the Smagorinsky model and also obtained results with a premature detachment of the boundary layer for lowes angle of attack.

**4.3 Coupling between integral and differential formulations**

The final proposal of this work is the coupling between the both formulations, where the data obtained in the simulation, drag  $C_d$  and lift  $C_l$  coefficient, are used to calculate the efficiency of the turbine using the integral formulation.

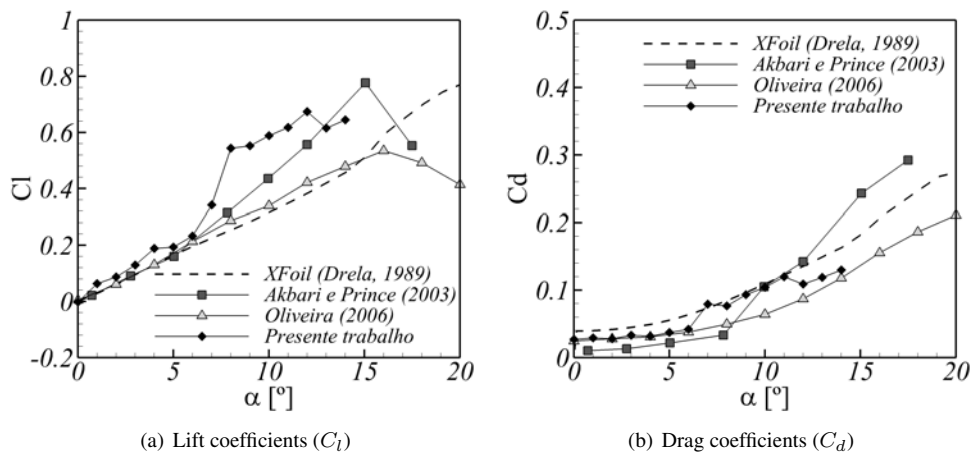


Figure 15. Lift and Drag coefficients in function of the angle of attack  $\alpha$  using the Van Driest function.

The Fig. 16 shows the power coefficient using simulation data and experimental data (Sheldahl and Klimas, 1981) for the NACA 0012 profile. It's used the geometric data of the turbine OWW (Leite and Araújo, 2007), presented in the results of the integral formulation. It's utilized Reynolds number  $Re = 10^4$ . And it's chosen an operating range of the turbine with  $t_{sr}$  varying from 0.2 to 3.2.

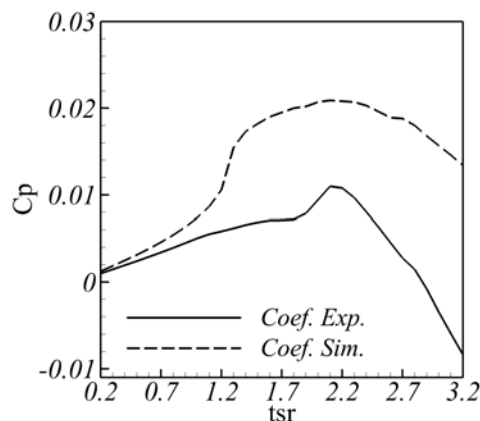


Figure 16. Comparison of the power coefficient using simulation and experimental data (Sheldahl and Klimas, 1981).

Using the data obtained from the numerical simulation performed in this work, results in a difference in the curves of the Fig. 16, once the lift coefficient was higher than the literature data, resulting a power  $C_p$  with greater values. It is also observed that the power coefficient is very low compared with the theoretical maximum value of the power coefficient for this type of turbine, which can reach the  $C_p = 0.59$  (Betz, 1928). This low efficiency is due to the fact that the Reynolds number is low for this type of application. Then it's necessary correct the causes of the numerical deviations present in the simulations with high values of Reynolds number. However, this result exemplifies the proposed coupling of the two formulations, integral and differential methods.

## 5. CONCLUSION

Wind energy is part of the solution to the world's energy demand. Computational analysis applied in wind turbines is remarkably versatile, once there are high costs in the laboratory, prototypes and experimental analysis. With the computational analysis it's possible to change the variables of the problem in search of the best solution for a specific problem.

With the integral formulation of wind rotor it's easily determine the efficiency of the turbine, once it is possible to calculate the forces acting on the blades of the rotor as a function of input variables of the model, which are wind speed, angular velocity of the rotor, length and the type of airfoil of the blade.

In the differential formulation was simulated two-dimensional flow over the NACA 0012 profile with high Reynolds number and has detected a premature separation of the boundary layer. The results for angle of attack less than 6 degrees remained close to literature data, but for higher angles occurs the premature detachment of the boundary layer. A bigger refinement in the mesh could solve this problem, as well as the use of averages equations or hybrid models *Detached Eddy*

R. R. S. Melo, J. M. Vedovoto and A. Silveira Neto  
Integral and Differential Formulations Applied to Analysis Flow Over a Wind Rotors

#### *Formulation - DES.*

Finally, this paper presents the coupling between integral and differential methods, showing that it is possible to solve a complex engineering problem with mathematical and numerical models, eliminating the necessity for experimental data.

To continue this work is necessary studies on the phenomenology of the interaction between turbulence and wall, coupled with the immersed boundary method, through the numerical simulation of turbulent flows using methodologies URANS, LES and Hybrid, such as DES .

#### **6. ACKNOWLEDGEMENTS**

To CAPES, CNPq, FAPEMIG and PETROBRAS for financial support.

#### **7. REFERENCES**

- Akbari, M. and Price, S., 2003. "Simulation of dynamic stall for a naca 0012 airfoil using a vortex method". *Journal of Fluids and Structures*, Vol. 17, No. 6, pp. 855 – 874. ISSN 0889-9746.
- Betz, A., 1928. "Windmills in the light of modern research". Technical report, National Advisory Committee for Aeronautics, Washington, EUA.
- Drela, M., 1989. "Xfoil : An analysis and design system for low reynolds number airfoils". *Lecture Notes in Engineering : Low Reynolds Number Aerodynamics*.
- Ferziger, J. and Peric, M., 1996. "Computational methods for fluid dynamics". *Springer*.
- Lanzafame, R. and Messina, M., 2010. "Horizontal axis wind turbine working at maximum power coefficient continuously". *Renewable Energy*, Vol. 35, No. 1, pp. 301 – 306. ISSN 0960-1481.
- Leite, G.N.P. and Araújo, A.M., 2007. "Modelagem dinâmica de conversão eólico mecânica em turbinas eólicas de eixo horizontal". *8 Congresso Iberoamericano de Engenharia Mecânica*.
- Melo, R.R.S. and Silveira-Neto, A., 2012. "Integral analysis of rotors of a wind generator". *Renewable and Sustainable Energy Reviews*.
- Oliveira, J.E.S., 2006. *Modelagem matemática para otimização dinâmica de corpos imersos em escoamentos turbulentos*. Ph.D. thesis, Universidade Federal de Uberlândia.
- Sedaghat, A. and Mirhosseini, M., 2012. "Aerodynamic design of a 300kw horizontal axis wind turbine for province of semnan". *Energy Conversion and Management*, Vol. 63, No. 0, pp. 87 – 94.
- Sheldahl, R.E. and Klimas, P.C., 1981. "Aerodynamic characteristic of seven symmetrical airfoil sections through 180 degree angle of attack for use in aerodynamic analysis of vertical axis wind turbines". Technical Report SAND 80 2114, EUA, Sandia National Laboratories, Albuquerque, NM, EUA.
- VanDriest, E.R., 1956. "On turbulent flow near a wall". *Journal of the Aeronautical Sciences*, Vol. 23, No. 11, pp. 1007 – 1011.

#### **8. RESPONSIBILITY NOTICE**

The authors are the only responsible for the printed material included in this paper.